JOURNAL OF AIRCRAFT
Vol. 39, No. 1, January–February 2002

Airfoil Validation Using Coupled Navier–Stokes and e^N Transition Prediction Methods

Hans W. Stock*
DLR, German Aerospace Center, 38108 Braunschweig, Germany

Navier–Stokes airfoil computations coupled to e^N transition prediction are feasible, provided the limiting N factor is known beforehand. In the present study a procedure is outlined to validate free-transition airfoil experiments in wind tunnels for which the limiting N factor is not known a priori. The approach does not rely on mesh adaption procedures to obtain adequate laminar viscous layer data from Navier–Stokes computations for the stability analysis. To the contrary, the laminar viscous layer is computed by a boundary-layer method applying as input the pressure distribution from Navier–Stokes computations on initial meshes. Two measurement campaigns are validated: the NLF(1)-0416 laminar airfoil in the low-speed NASA Langley Low-Turbulence Pressure Tunnel LTPT and the NACA 64_2A015 airfoil in the NASA Ames 12-Foot Pressure Tunnel. The free-transition measurements in both tunnels include pressure distributions and transition locations and, in supplement, for the NLF(1)-0416 laminar airfoil lift and drag measurements. The computational results document the validity of the present approach, the existence of a constant limiting N factor for a specific wind tunnel, and an excellent agreement with the experimental findings.

Nomenclature

C	=	chord length
C_D	=	drag coefficient
C_L	=	lift coefficient
C_M	=	moment coefficient
C_p	=	pressure coefficient
c_f	=	skin-friction coefficient
c_p	=	pressure coefficient
M	=	freestream Mach number
N	=	N factor
$N_{\max}$	=	envelope of the N factor curves of unstable waves
Re	=	Reynolds number based on chord and freestream conditions
X	=	coordinate in freestream direction
X_{Tr}	=	X value at transition
α	=	angle of attack

Introduction

THE laminar flow technology is one of the major technologies in aeronautics that offers a large potential of improvements for future commercial transport aircraft concerning the reduction of fuel consumption and take-off weight and the significant amelioration of cruise lift-to-drag ratio. To evaluate potential savings in fuel costs or improvements in aerodynamic efficiency as a function of laminar surface area, one must be able to predict accurately the location of boundary-layer transition on wings and nacelles.

It is commonly accepted that transition is the result of complex phenomena, which depend on many parameters, such as Reynolds number, pressure sgradient, wall temperature, wall mass transfer, disturbance environment, etc. The first stage of the transition process is characterized by the boundary-layer receptivity. This process desribes the means by which the environmental disturbances (freestream turbulence, noise, vibration, surface roughness and waviness, etc.) trigger the laminar boundary layer to develop mechanisms that lead to transition. The way in which the initialized disturbances grow can be described by two different processes. First, if the amplitudes of the initialized disturbances are small they are amplified linearly up to the point where transition occurs (natural transition); second, if the initialized disturbances are not weak nonlinear phenomena are immediately observed, transition occurs rapidly, and the linear growth of the disturbances is bypassed (bypass transition). Furthermore, the phenomenon of attachment line transition cannot be described by the linear growth of disturbances, either.

On one hand, a rigorous modeling of the transition process is up to now not available. On the other hand, the so-called e^N method,[1,2] which is based on linear theory of parallel flows, does not account for some fundamental aspects of the transition process, but nevertheless represents the most frequently used transition prediction method today. Concluding, any criticism of the reliability of the e^N method should be based on the fact that there is no other practical method presently available for industrial applications.[3]

Only recently, the problem of coupling two-dimensional Navier–Stokes codes with the e^N method has been tackled.[4–8] In Ref. 7 a feasibility study is performed, which describes in detail the necessary steps required to obtain via a mesh adaption procedure reliable Navier–Stokes results for the stability analysis. This includes the determination of the viscous-layer outer edge in the laminar and turbulent flow regimes with a sufficiently large and, more importantly, a constant number of mesh points in the wall normal direction inside the viscous layer. The necessity to include transition zone computations in order to produce stable, converged solutions is documented and the transition zone modeling outlined in Ref. 8. The experimental findings on the DoAl3 laminar airfoil, which was tested in the Transonic Wind Tunnel of the DLR in Braunschweig, Germany,[9] have been successfully validated by computations.[7,8] The transition locations on the DoAl3 airfoil were not determined in the course of the free-transition measurements; the limiting N factor of the TWB was evaluated beforehand.[10]

For design purposes the unique limiting N factor can be applied, which was determined from free flight experiments,[11–15] contrary to the validation of experiments in a wind tunnel for which a specific and constant limiting N factors exists, which depends mainly on the disturbance environment. The concern of the present study is related to the validation of laminar airfoil experiments for which the limiting N factor of the wind tunnel is a priori not known. It will be shown that the same computational procedure of Refs. 7 and 8 is applicable, if the transition locations on the airfoil are obtained experimentally.

Received 13 April 2001; revision received 10 July 2001; accepted for publication 5 September 2001.

*Senior Research Scientist, Institute of Aerodynamics and Flow Technology, Lilienthal-platz 7.

The NLF(1)-0416 laminar airfoil[16] and the NACA 64_2A015 airfoil[17] are chosen for validation, tested in the low-speed NASA Langley Low-Turbulence Pressure Tunnel LTPT and in the NASA Ames 12-Foot Pressure Tunnel, respectively. The transition locations on the NLF(1)-0416 laminar airfoil were measured for a Reynolds number $Re = 2.0 \times 10^6$ on upper and lower surface for 25 values of the angle of attack from $\alpha = -14$ to 14 deg. Futhermore, for Reynolds numbers $Re = 1 \times 10^6$ and 4×10^6 transition locations were measured for different angles of attack, $\alpha = -1$, 1, 4, and 6.1 deg. In supplement, surface pressures for $Re = 4 \times 10^6$ and lift and drag values are reported in Ref. 16 for all Reynolds numbers just mentioned. The transition locations and surface pressures on the NACA 64_2A015 airfoil[17] were measured on the upper airfoil surface for three angles of attack, $\alpha =$ 0, 0.5 and 1 deg, and for Reynolds numbers ranging from 10 to 40×10^6.

Applied Computational Methods

It is shown in Ref. 7 that the Navier–Stokes code delivers reliable laminar viscous-layer results only if the computations are executed on adapted meshes. To the contrary, the airfoil pressure distributions, forces, and moments computed by the Navier–Stokes code are almost independent on whether the computations are produced on initial or adapted meshes.[7] On one hand, the N factors evaluated from Navier–Stokes solutions for laminar viscous layers on initial meshes differ considerably from those evaluated from the corresponding boundary-layer solution; the pressure distribution of the Navier–Stokes solution on initial meshes is used as input to the boundary-layer computation. On the other hand, for a viscous adapted mesh the Navier–Stokes and boundary-layer N factors are identical.[7] Furthermore and more importantly, the stability results based on boundary-layer computations using as input the Navier–Stokes pressure distributions computed on initial and adapted meshes are also identical. Hence, the Navier–Stokes computations can be applied without any loss of accuracy on initial meshes. The time-consuming process of mesh adaption is no longer required; the laminar viscous-layer results for the stability analysis are furnished by boundary-layer computations instead.

The coupling of the Navier–Stokes method with the e^N method consequently applies three different codes for the iterative computation cycle:

1) The Reynolds-averaged Navier–Stokes equations, describing two-dimensional, unsteady, compressible flows in conservation form, are solved by means of a finite volume approach using a Runge–Kutta time-stepping method with multigrid acceleration.[18] The Johnson–King turbulence model in its original form[19] is applied in the transitional and turbulent flow regimes.

2) The boundary-layer method for laminar, compressible flows on swept, tapered wings[20] is a finite difference method with second-order accuracy in marching and fourth-order accuracy in wall normal direction, hence being free of any numerical viscosity, in contrast to the Navier–Stokes method.

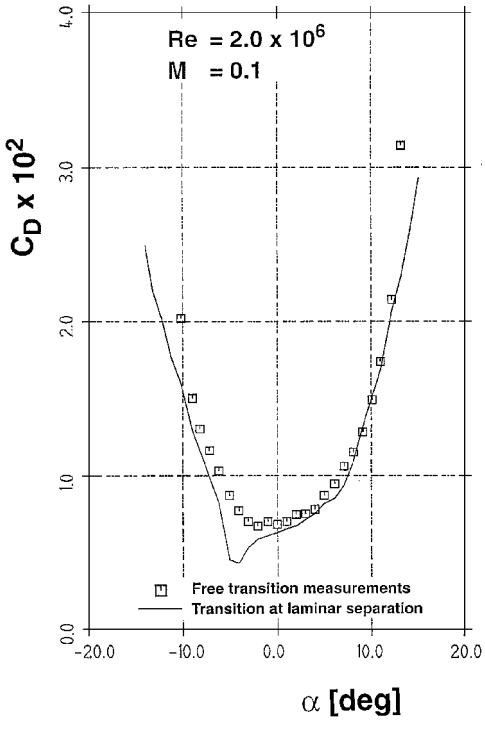

Fig. 1 Free-transition drag measurements for the NLF(1)-0416 laminar airfoil compared to initial computations.

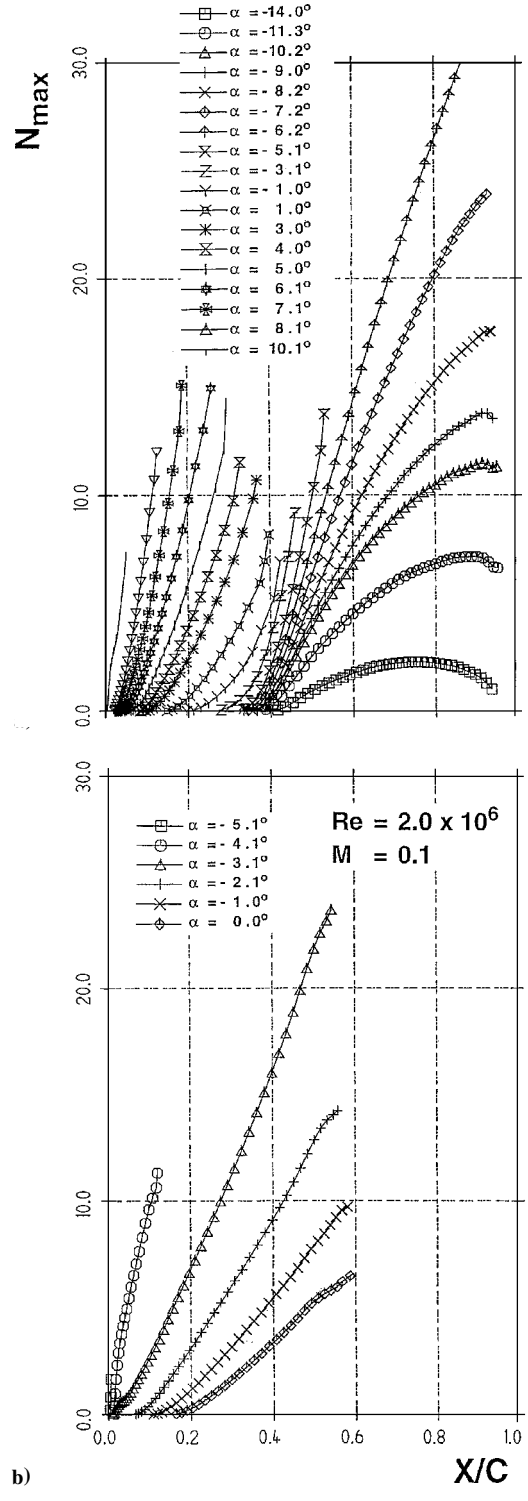

Fig. 2 N_{max} curves for the initial computations on a) upper and b) lower surface of the NLF(1)-0416 laminar airfoil.

3) The stability method[21] solves the three-dimensional, compressible Orr–Sommerfeld stability equations using a finite difference scheme.

All Navier–Stokes computations are carried out using four mesh levels for the multigrid procedure with 512×128 mesh volumes. The grid dependence of the Navier–Stokes results of the NLF(1)-0416 airfoil is documented in Table 1 for an angle of attack $\alpha = 0$ deg, a Mach number $M = 0.1$, and a Reynolds number $Re = 2 \times 10^6$. The grid dependence results are very similar to those for the DoAl3 airfoil reported in Ref. 7.

Table 1 Grid dependence of the Navier–Stokes method

Grid points	C_D	C_L	C_M
64×16	−0.0019348	−0.13687	0.10926
128×32	0.011407	0.50312	−0.11286
256×64	0.0066722	0.50979	−0.11356
512×128	0.0062737	0.49664	−0.11061
1024×256	0.0062394	0.49611	−0.11039

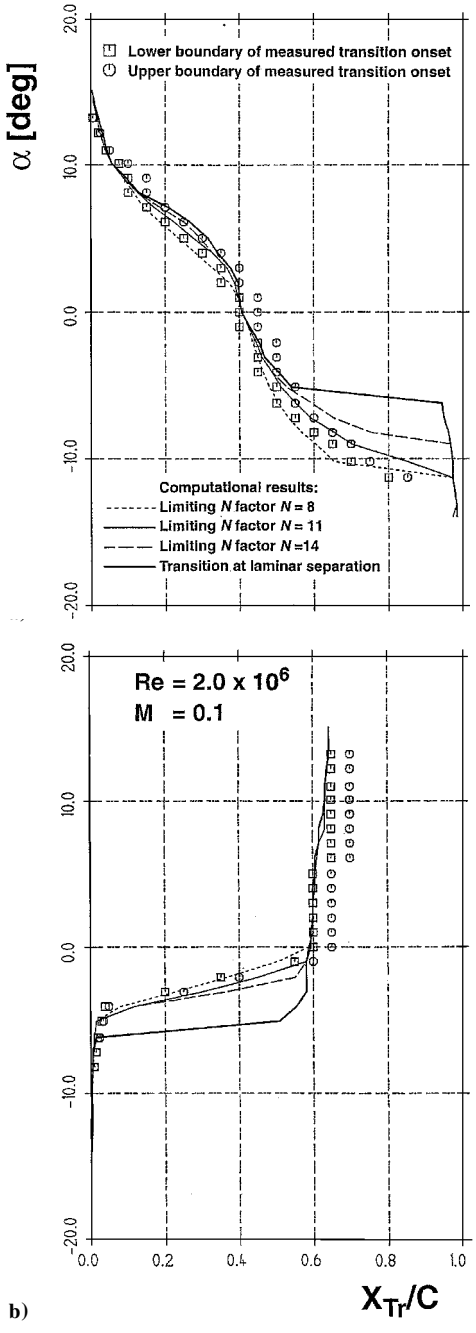

Fig. 3 Measured transition locations on a) upper and b) lower surface of the NLF(1)-0416 laminar airfoil compared to initial and final computations for different limiting N factors.

Computational Procedure of the Coupled Methods

The iterative computation cycle is started performing a Navier–Stokes run with point transition fixed right before laminar separation on an initial mesh. The laminar separation point is updated continously in the course of the time stepping Navier–Stokes computations. Transition is then fixed one mesh point upstream of the separation point. Hence, the transition point on both airfoil surfaces for the subsequent iterations will be moved upstream only. The laminar boundary-layer development[20] is computed and analyzed with the linear stability code applying the incompressible analysis.[21] Unstable Tollmien–Schlichting waves are computed for a perturbation propagation direction $\Psi = 0$, i.e., in direction of the inviscid outer flow, whose amplification rates deliver the N factor distributions for constant, unstable frequencies. On one hand, the envelope of the N curves, N_{max}, marks a specific location, where the the limiting N factor is exceeded. Experience teaches

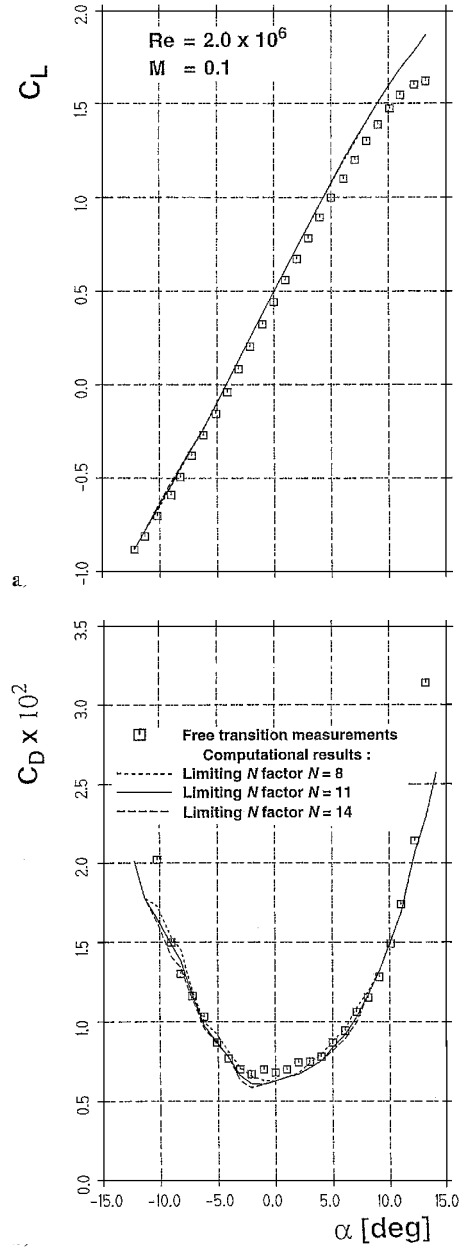

Fig. 4 Measured a) lift and b) drag polars of the NLF(1)-0416 laminar airfoil compared to final computations applying different limiting N factors.

that transition can be assumed to have occured at that location.[10–15] On the other hand, if the N_{max} values remain below the limiting N factor the transition location remains fixed right before laminar separation. The newly computed transition locations on upper and lower surface are then transferred in a slightly underrelaxed manner to the subsequent Navier–Stokes run on the same initial mesh, applying now the transition zone modeling.[8] The newly updated transition locations are evaluated applying the computational steps just mentioned. Usually the third iteration cycle delivers a converged solution.

Results

NLF(1)-0416 Laminar Airfoil

The low-speed NLF(1)-0416 laminar airfoil is designed for high maximum lift with a relatively large nose radius for which minimum drag is not required to be constant above a certain value of lift, and low drag is not required below cruise lift. It is shown in Ref. 16 that the transition point on the upper surface of the NLF(1)-0416 laminar airfoil moves steadily toward the leading edge with increasing angle of attack, as opposed to the sudden jump characteristic on both surfaces of the DoAL3 laminar airfoil,[7,8] which forms a distinct laminar bucket.

$Re = 2 \times 10^6$

The measured drag values are compared in Fig. 1 with the results of the initial Navier–Stokes solutions where point transition is applied at laminar separation. As can be seen in the region of small negative values of the angle of attack, the drag is considerably underpredicted compared to the measurements as a result of an overestimate of the laminar flow regions on both airfoil surfaces. The envelopes of the N curves N_{max} on the upper and lower surface, respectively, are presented for different angles of attack in Fig. 2. On the upper airfoil surface stability results are obtained for the complete range of the angle of attack contrary to the lower airfoil surface flows. On the lower surface laminar separation is indicated right at the nose for values of the angle of attack below $\alpha = -5.1$ deg, where transition is imposed, and for values above $\alpha = 0$ deg the flow is completely stable.

The limiting N factor of the low-speed NASA Langley Low-Turbulence Pressure Tunnel (LTPT) is a priori not known and has to be determined based on the transition location measurements on the upper and lower airfoil surface (Fig. 3). The transition locations of the initial Navier–Stokes solutions, which are identical to the laminar separation points, are represented as the thick line in Fig. 3. As can be seen, the laminar flow regions are slightly overpredicted on the upper surface for angles of attack, $\alpha = 4$ to 8 deg, and for values of $\alpha = -6$ to -10 deg the laminar flow extent is drastically overestimated, similarly on the lower surface for values of $\alpha = -2$ to -5 deg. A close inspection of the stability data (Fig. 2)

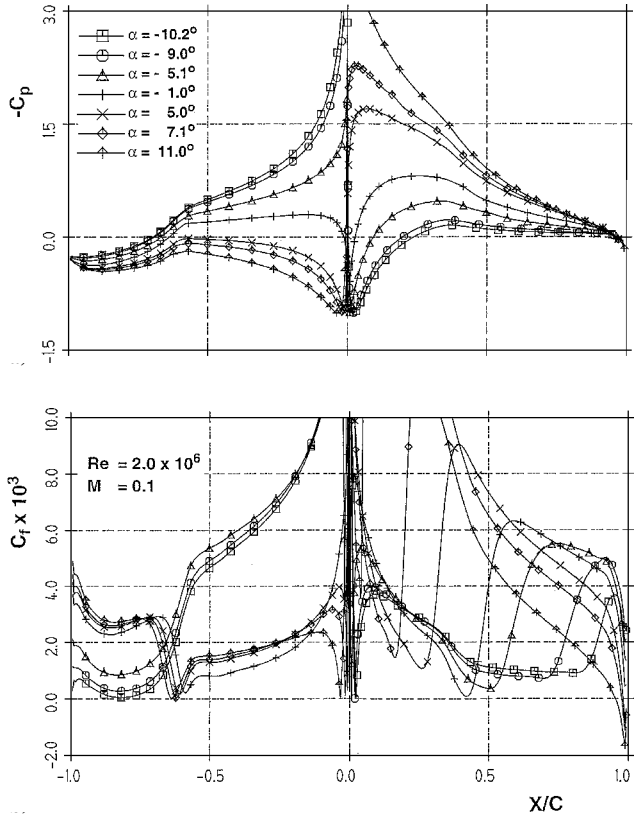

Fig. 5 Distributions of a) computed pressure and b) skin friction on the NLF(1)-0416 laminar airfoil for different angles of attack and a limiting N factor of 11.

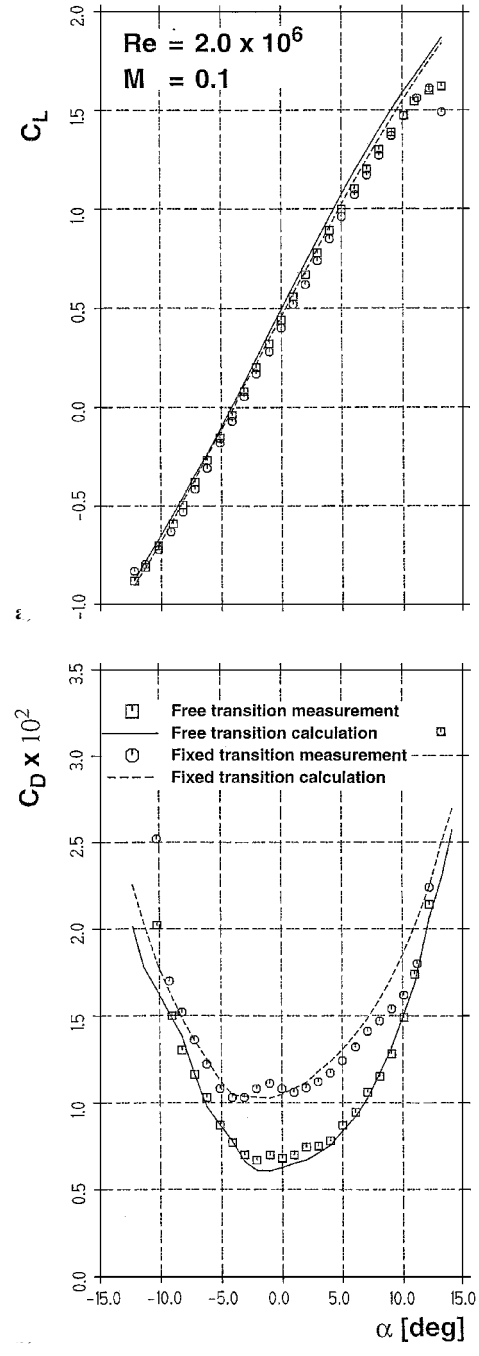

Fig. 6 Measured and computed a) lift and b) drag of the NLF(1)-0416 laminar airfoil for fixed and free transition applying a limiting N factor 11.

and the measured transition locations (Fig. 3) suggests the limiting N factor to lie in between $N = 8$–14. Three different values for the limiting N factor—$N = 8$, 11, and 14—are tested numerically. The results of the iteratively converged computations for all measured angles of attack and the different limiting N factors are depicted in Fig. 3. As can be seen, the best agreement between measurements and computations is obtained for the specific and constant limiting N factor of 11. Figure 4 shows the final iterated results of the lift and drag polars evaluted for the different limiting N factors compared to measurements. The overall agreement is excellent apart from the fact that the lift is slightly overpredicted for large positive angles of attack. The differences in the lift polar for the different limiting N factors are almost neglible; small differences in the predicted drag are observed obviously producing the smallest drag values for the largest limiting N factor.

For some values of the angle of attack, $\alpha = -10$ to 11 deg, the computed pressure and skin-friction distributions are depicted for converged Navier–Stokes solutions and a limiting N factor of 11 (see Fig. 5). Positive values of X/C indicate the upper and negative values of the lower airfoil surface. The skin-friction coefficient is the only viscous-layer property, which is almost identical for Navier–Stokes computations on initial and adapted meshes.[7] As can be seen, the pressure distributions do not exhibit local perturbations at the transition location because of the introduction of transitional flow computations.[8] Flow situations where the vanishing laminar skin-friction indicates the approach to separation describe viscous layers for which the N_{max} factors show values below the limiting N factor. The variation of the skin-friction coefficient between fully laminar and fully turbulent flow on the upper airfoil surface shows clearly the influence of the different lengths of the transition zone imposed by the modeling.[8] The increase from laminar to turbulent friction is progressively less pronounced when transition is predicted further downstream. Finally, the difference in lift and drag for free and forced transition measurements is shown in Fig. 6. Transition was fixed in the experiments at 7.5% chord on both airfoil surfaces[16]; the free-transition computations apply a limiting N factor of 11. For both measurements and computations the lift is slightly larger in the free-transition case for which the boundary layers on both surfaces are thinner reducing the decambering effect of the viscous layers. The agreement of measured and predicted drag (Fig. 6) is shown to be excellent for both flow situations.

$Re = 1 \times 10^6$ and 4×10^6

Pressure distributions are reported in Ref. 16 for a Reynolds number of 4×10^6 and transition location measurements for Reynolds numbers 1×10^6 and 4×10^6 and angles of attack from $\alpha = -1$ to 6.1 deg. Figure 7 gives as an example for one angle of attack the computed pressure distributions of iterated Navier–Stokes solutions for the aforementioned Reynolds numbers applying a limiting N factor of 11. A slight lift increase is visible for increasing Reynolds numbers and, furthermore, for a Reynolds number of 4×10^6, the agreement with measurements is satisfactory. The slight disagreement,

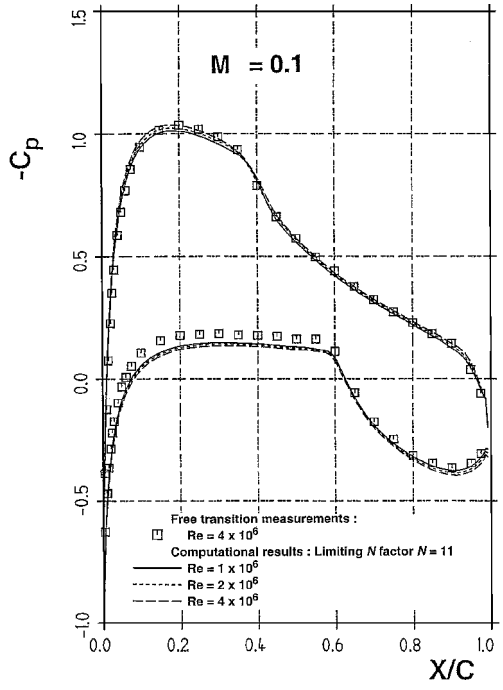

Fig. 7 Measured and predicted pressure distributions on the NLF(1)-0416 laminar airfoil for different Reynolds numbers, $\alpha = 1$ deg and a limiting N factor of 11.

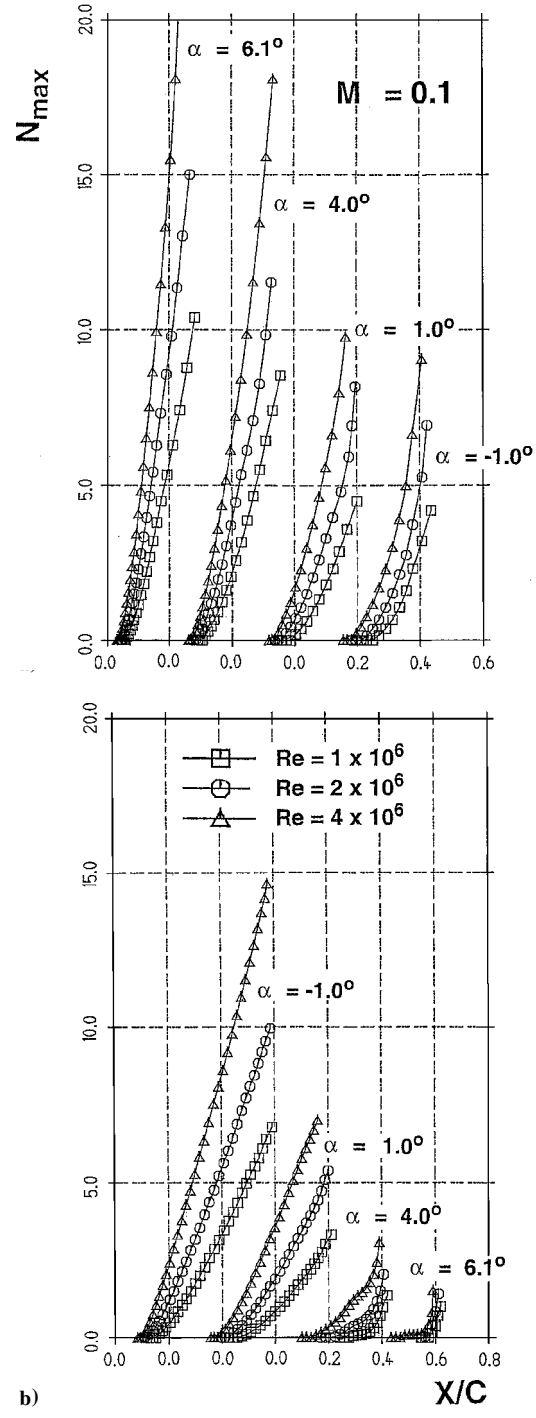

Fig. 8 N_{max} curves for the initial computations on a) upper and b) lower surface of the NLF(1)-0416 laminar airfoil for different Reynolds numbers and angles of attack.

clearly visible on the airfoil lower surface, is probably because a proper wind-tunnel correction would have indicated a mildly different angle of attack. The N-factor behavior for the initial Navier–Stokes solutions is described for the different Reynolds numbers and angles of attack on upper and lower airfoil surface in Fig. 8. Several features of the stability behavior can be detected:

1) The point of neutral stability (position where the perturbations in the flow first start to be amplified, i.e., where the N factor value equals zero) moves upstream on the upper airfoil surface if the angle of attack is increased, with a simultaneous growth of the N factors caused by the growing adverse pressure gradient in the recompression zone downstream of the minimum pressure, which destabilizes the laminar boundary-layer flow.

2) The point of neutral stability moves upstream on the lower airfoil surface with a simultaneous growth of the N factors, if the angle of attack is decreased.

3) Increased Reynolds numbers shift the point of neutral stability upstream and lead to larger N-factor values.

The prediction quality of the transition locations on both airfoil surfaces compared to measurements is shown in Fig. 9. As can be seen, the transition location is shifted slightly upstream on both upper and lower airfoil surfaces for increasing Reynolds number and upstream on the upper airfoil surface for increasing angles of attack and downstream on the lower surface, respectively. Finally, the lift and drag polars for the considered Reynolds numbers are shown in Fig. 10. The lift is increasingly overpredicted with respect to an increase of the angle of attack, but the predicted increment of lift increase caused by Reynolds-number augmentation is very similar to the experimentally observed increase. Similarly, the drag prediction is of satisfactory quality where the variation in drag caused by Reynolds-number increase is well captured by the computations.

NACA 64_2A015 Airfoil Section

To validate further the actual procedure measurements of Ref. 17 on an infinite swept wing are validated. Some experiments are reported on the zero sweep configuration for which wall-pressure distributions and transition locations were measured.[17] For constant angles of attack, $\alpha = 0, 0.5$, and 1 deg, the Reynolds number was varied from 10 to 40×10^6 at a constant Mach number, 0.27. Figure 11

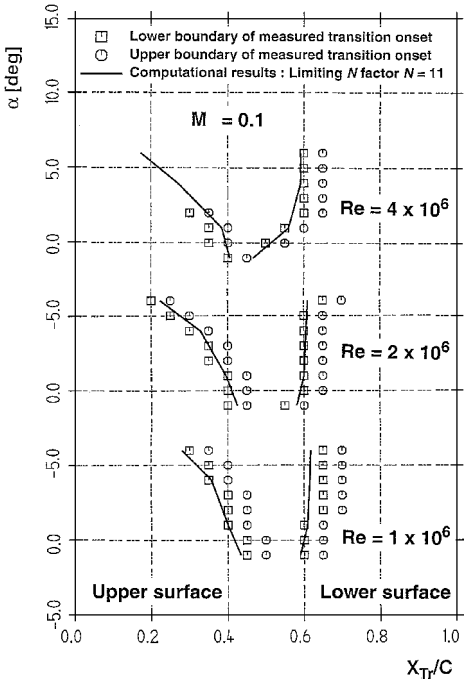

Fig. 9 Measured and predicted transition locations on the upper and lower surface of the NLF(1)-041 laminar airfoil for different Reynolds numbers and angles of attack.

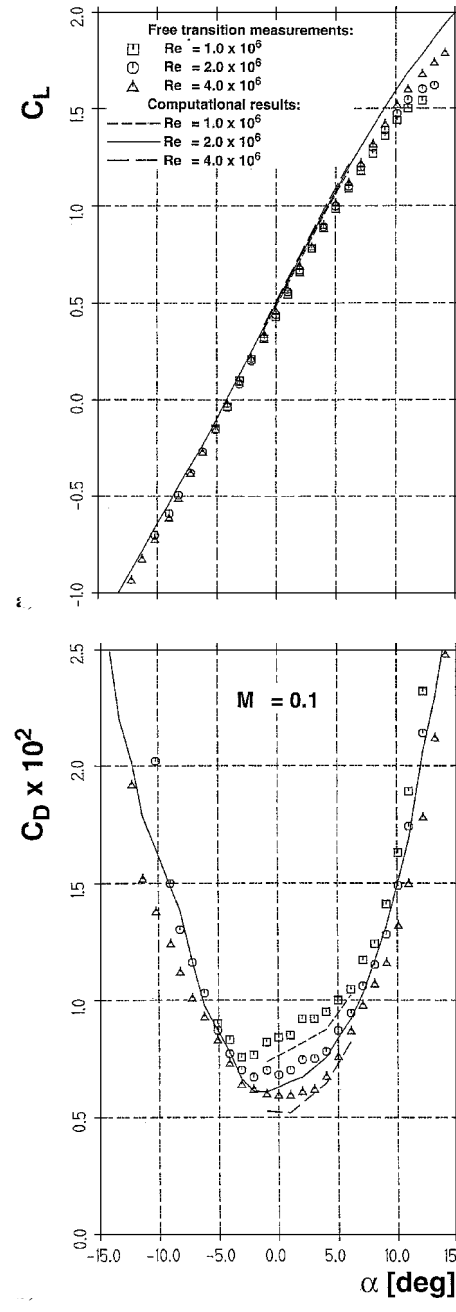

Fig. 10 Measured and computed a) lift and b) drag of the NLF(1)-0416 laminar airfoil for different Reynolds numbers and a limiting N factor of 11.

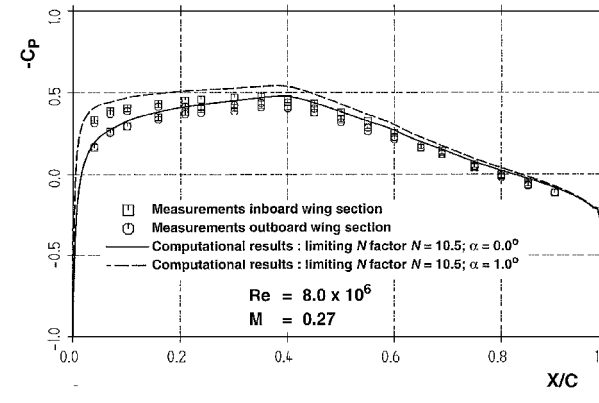

Fig. 11 Measured and predicted pressure distributions on the upper surface of the NACA 64_2A015 airfoil for two angles of attack.

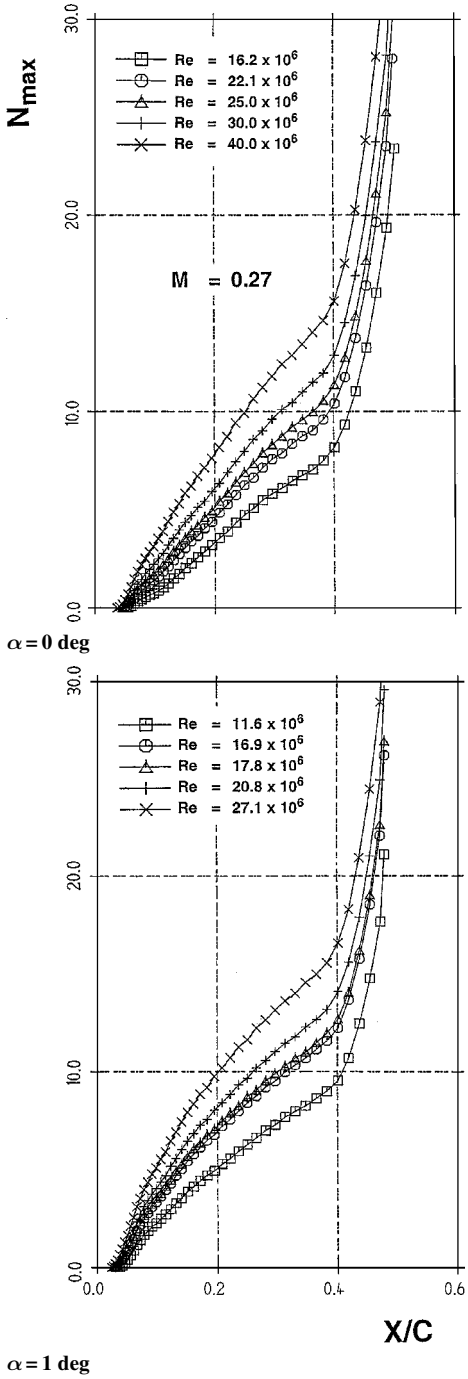

Fig. 12 N_{max} curves for the initial computations on the upper surface of the NACA 64_2A015 airfoil for two angles of attack.

shows the comparison of measured and computed wall pressure on the upper airfoil surface at $\alpha = 0$ and 1 deg. The measured data for the inboard and outboard wing section agree extremely well, indicating that the spanwise pressure gradient is negligibly small. The computed pressure is shown to be in fairly good agreement with the measurements. Figure 12 documents the upper surface stability data for two angles of attack. Here again, the increase of the Reynolds number shifts the neutral stability point slightly upstream and augments the N_{max} values. Similar to the preceeding measurement campaign, the limiting N factor, not known beforehand, is varied from $N = 9.5$ to 11.5. For three different values of the limiting N factor, the measured transition locations are compared to computations in Fig. 13. As can be seen for a limiting N factor 10.5, the measured and computed transition locations are in good agreement.

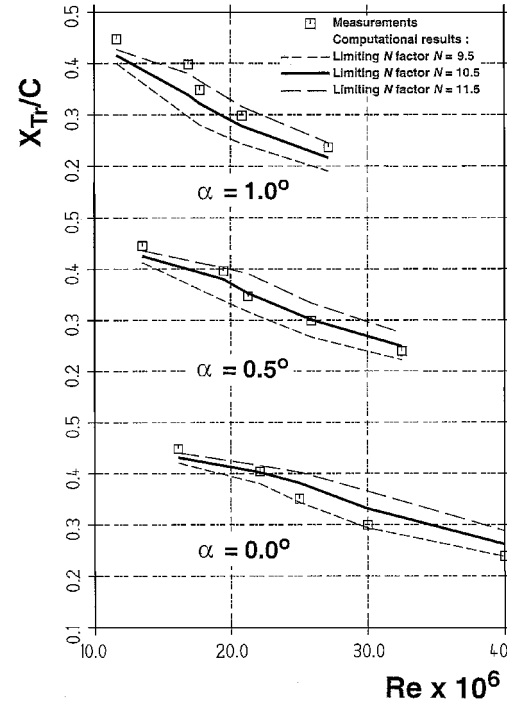

Fig. 13 Measured and predicted transition locations on the upper surface of the NACA 64_2A015 airfoil for different limiting N factors and angles of attack.

Conclusions

It is shown that a Navier–Stokes method for laminar airfoils is successfully coupled to the e^N method for the validation of free-transition experiments in wind tunnels for which the limiting N factors are not known a priori. The proposed coupling procedure avoids the time-consuming mesh-adaption procedure for Navier–Stokes solutions to obtain reliable laminar viscous-layer results. To the contrary, it is documented that the application of laminar boundary-layer computations for the stability analysis using the pressure distribution of Navier–Stokes solutions on initial meshes as input is feasible without any loss of accuracy.

The free-transition measurements on two airfoils, the NLF(1)-0416 laminar airfoil and the NACA 64_2A015 airfoil tested in the low-speed NASA Langley Low-Turbulence Pressure Tunnel and the NASA Ames 12-Foot Pressure Tunnel, respectively, show good agreement with the computational results. The specific limiting N factors of both tunnels not known beforehand are determined by a computational sensitivity study applying the measured transition locations. The required constancy of the limiting N factor for the considered wind tunnels is shown to be valid for a large varity of flow conditions, especially for the NLF(1)-0416 laminar airfoil. The measured transition locations agree excellently with the computations. In addition, the measured lift and drag values for the NLF(1)-0416 laminar airfoil are well predicted by the proposed approach, which includes also the comparison of lift and drag for fixed-transition measurements.

References

[1] Smith, A. M. O., and Gamberoni, N., "Transition, Pressure Gradient and Stability Theory," Douglas Aircraft Co., Calif. Rep. ES 26388, Long Beach, CA, Aug. 1956.

[2] van Ingen, J. L., "A Suggested Semi-Emperical Method for the Calculation of the Boundary Layer Transition Region," Univ. of Delft, Dept. of Aerospace Engineering, Rept. VTH-74, The Netherlands, Oct. 1956.

[3] Arnal, D., and Casalis, G., "Laminar-Turbulent Transition Prediction in Three-Dimensional Flows," *Progress in Aerospace Sciences*, Vol. 36, 2000, pp. 173–191.

[4] Radespiel, R., Graage, K., and Brodersen, O., "Transition Predictions Using Reynolds-Averaged Navier–Stokes and Linear Stability Analysis Methods," AIAA Paper 91-1641, June 1991.

[5]Garriz, J. A., Vatsa, V. N., and Sanetrik, M. D., "Issues Involved in Coupling Navier–Stokes Mean-Flow and Linear Stability Codes," AIAA Paper 94-0304, Jan. 1994.

[6]Ramakrishnan, R., Vatsa, V. N., Otto, J., and Kumar, A., "A Detailed Study of Mean-Flow Solutions for Stability Analysis of Transitional Flow," AIAA Paper 93-3052, Aug. 1993.

[7]Stock, H. W., and Haase, W., "A Feasibilty Study of e^N Transition Prediction in Navier–Stokes Methods for Two Dimensional Airfoil Computations," *AIAA Journal*, Vol. 37, No. 10, 1999, pp. 1187–1196.

[8]Stock, H. W., and Haase, W., "Navier–Stokes Airfoil Computations with e^N Transition Prediction Including Transitional Flow Regions," *AIAA Journal*, Vol. 38, No. 11, 2000, pp. 2059–2066.

[9]Müller, R., Puffert-Meißner, W., and Lück, H., "Messungen am Laminarprofil DoAL3 im Transsonischen Windkanal Braunschweig (TWB)," DLR-Interner Bericht, DLR, German Aerospace Establishment, Rept. IB 129-87/9, Braunschweig, Germany, 1987.

[10]Köster, H., and Müller, R., "Bestimmung des N-Faktors im Transsonischen-Windkanal Braunschweig (TWB) anhand von Druckverteilungs- und Umschlagspunkt messungen und dem Sally-Verfahren," *6th DGLR-Fach-Symposium (Strömungen mit Ablösung)*, edited by Deutsche Gesellschaft für Luft- und Raumfahrt e.V. (DGLR), 8-9.11.1988, DGLR-REP. 88-05, Braunschweig, Germany, 1988, pp. 66–77.

[11]Schrauf, G., "Transition Prediction Using Different Linear Stability Analysis Strategies," AIAA Paper 94-1848, June 1994.

[12]Henke, R., and Münch, F. X., "Natural Laminar Flow: A Wind Tunnel Test Campaign and Comparison with Free Flight Test Data," AIAA Paper 90-3045, Aug. 1990.

[13]Horstmann, K. H., Redeker, G., Quast, A., Dressler, U., and Bieler, H., "Flight Tests with a Natural Laminar Flow Glove on a Transport Aircraft," AIAA Paper 90-3044, Aug. 1990.

[14]Schrauf, G., Perraud, J., and Lam, F., "Comparison of Boundary Layer Transition Predictions Using Free Flight Test Data," *Journal of Aircraft*, Vol. 35, No. 6, 1998, pp. 891–897.

[15]Schrauf, G., "Linear Stability Theory Applied to Wind Tunnel and Flight Experiments," *Proceedings of the 4th European Computational Conference*, Vol. 2, Wiley, Chichester, United Kingdom, 1998, pp. 126–131.

[16]Somers, D. M., "Design and Experimental Results for a Natural-Laminar-Flow Airfoil for General Aviation Applications," NASA TP 1861, April 1981.

[17]Boltz, F. W., Kenyon, G. C., and Allen, C. Q., "Effects of Sweep Angle on the Boundary-Layer Stability Characteristics of an Untapered Wing at Low Speeds," NASA TN D-338, Oct. 1960.

[18]Haase, W., "EUROVAL—A European Initiative on Validation of CFD Codes," *Notes on Numerical Fluid Mechanics*, Vol. 42, Braunschweig, Vieweg, 1992, pp. 82–87.

[19]Johnson, D. A., and King, L. S., "A Mathematical Simple Turbulence Closure Model for Attached and Separated Turbulent Boundary Layers," *AIAA Journal*, Vol. 23, No. 11, 1985, pp. 1684–1692.

[20]Horton, H. P., and Stock, H. W., "Computation of Compressible, Laminar-Boundary Layers on Swept, Tapered Wings," *Journal of Aircraft*, Vol. 32, No. 6, 1995, pp. 1402–1405.

[21]Schrauf, G., "An Efficient Solver of the Eigenvalue Problem of the Linear-Stability Equations for Three-Dimensional, Compressible Boundary Layer Flows," *6th DGLR-Fach-Symposium (Strömungen mit Ablösung)*, edited by Deutsche Gesellschaft für Luft- und Raumfahrt e.V. (DGLR), 8-9.11.1988, DGLR-REP. 88-05, Braunschweig, Germany, 1988, pp. 18–27.